

Atomistic Study of the Lattice Thermal Conductivity of Rough Graphene Nanoribbons

Hossein Karamitaheri, Mahdi Pourfath, *Member, IEEE*, Rahim Faez, and Hans Kosina, *Member, IEEE*

Abstract—Following our recent study on the electronic properties of rough nanoribbons [1], in this paper the role of geometrical and roughness parameters on the thermal properties of armchair graphene nanoribbons is studied. Employing a fourth nearest-neighbor force constant model in conjunction with the nonequilibrium Green's function method the effect of line-edge-roughness on the lattice thermal conductivity of rough nanoribbons is investigated. The results show that a reduction of about three orders of magnitude of the thermal conductivity can occur for ribbons narrower than 10 nm. The results indicate that the diffusive thermal conductivity and the effective mean free path are directly proportional to the ribbon's width and the roughness correlation length, but inversely proportional to the roughness amplitude. Based on the numerical results an analytical model for the thermal conductivity of narrow armchair graphene nanoribbons is proposed in this paper. The developed model can be used in the analysis of graphene-based nano transistors and thermoelectric devices, where the appropriate selection of geometrical and roughness parameters are essential for optimizing the thermal properties.

Index Terms—Correlation length, graphene nanoribbons (GNRs), line-edge-roughness (LER), roughness parameters, thermal conductivity.

I. INTRODUCTION

THERMAL properties of nanostructures are recently investigated as they are of interest for nanoelectronic and thermoelectric applications. A high thermal conductivity is beneficial for thermal management and nanoelectronic devices, in which hot spots, caused by heat dissipation in a relatively small volume, need to be cooled down [2], [3]. On the other hand, the performance of thermoelectric devices is inversely proportional to the thermal conductivity. A low thermal conductivity is, therefore, required for these devices [4], [5].

Graphene, a recently discovered form of carbon, has received much attention over the past few years because of

its excellent electrical, optical, and thermal properties [6]. A linear dispersion around the Dirac point and extremely high carrier mobility render graphene a promising material for optical and electronic applications [7]–[10]. Experimental studies have also reported a high Seebeck coefficient in graphene-based devices [11], [12]. In addition, a high thermoelectric performance is theoretically predicted in some graphene-based structures [13], [14] by degrading the extraordinary ability of pristine graphene to conduct heat [2]. The high thermal conductivity of graphene is mostly because of the lattice contribution, whereas the electronic contribution to the thermal conduction is negligibly small [15]–[18]. Therefore, by proper engineering of phonon transport a relatively high or a low thermal conductivity, as needed by a specific application, can be achieved.

As a zero bandgap material, pristine graphene can neither be used as a semiconducting channel in transistors nor as a thermoelectric material, because of its very small Seebeck coefficient [19]. However, one can open up a band-gap by appropriate patterning of the graphene sheet [20]–[22]. Graphene nanoribbons (GNRs) are thin strips of graphene, where the bandgap depends on the chirality of the edges and the width of the ribbon. Zigzag GNRs show metallic behavior, whereas armchair GNRs (AGNRs) are semiconductors with a bandgap inversely proportional to the width [20]. To obtain a bandgap of 0.5 eV, the width of the AGNR should be scaled down to around 3 nm. However, it is shown that boundaries and edge roughness can strongly influence the electrical and thermal properties of such narrow ribbons [23]–[26].

Recently, the electrical properties and device performance of AGNR-based field-effect transistors in the presence of line-edge-roughness (LER) and electron-phonon scattering are studied [1], [27]–[31]. On the other hand, several studies are recently conducted on the thermal properties of rough GNRs [32]–[37]. However, LER in these studies is modeled by either employing a specularly parameter [33], [36], [37] or randomly removing atoms along the edge chains [32], [35]. In addition, recent experimental studies on the thermal conductivity of silicon nanowires have demonstrated that besides the root mean square (rms) of the roughness amplitude, the roughness correlation length can also influence the thermal conductivity [38], [39]. Therefore, in this paper we use an exponential autocorrelation function to model the LER, which captures more details of realistic edges [1]. We numerically study the effects of the ribbon's geometrical parameters as well as roughness parameters, to show how these parameters can be used for engineering the thermal properties.

This paper is organized as follows. In Section II, the model and the methodology are explained. In Section III,

Manuscript received February 21, 2013; revised April 13, 2013; accepted May 2, 2013. Date of publication June 4, 2013; date of current version June 17, 2013. This work was supported by the European Commission under Grant 263306. The review of this paper was arranged by Editor R. Venkatasubramanian.

H. Karamitaheri is with the Institute for Microelectronics, Technische Universität Wien, Wien A-1040, Austria, and also with the School of Electrical Engineering, Sharif University of Technology, Tehran 14395-515, Iran (e-mail: karamitaheri@iue.tuwien.ac.at).

M. Pourfath is with the School of Electrical and Computer Engineering, University of Tehran, Tehran 14395-515, Iran, and also with the Institute for Microelectronics, Technische Universität Wien, Wien A-1040, Austria (e-mail: pourfath@iue.tuwien.ac.at).

R. Faez is with the School of Electrical Engineering, Sharif University of Technology, Tehran 14395-515, Iran (e-mail: faez@ee.sharif.ac.ir).

H. Kosina is with the Institute for Microelectronics, Technische Universität Wien, Wien A-1040, Austria (e-mail: kosina@iue.tuwien.ac.at).

Color versions of one or more of the figures in this paper are available online at <http://ieeexplore.ieee.org>.

Digital Object Identifier 10.1109/TED.2013.2262049

the results are presented and discussed. The effect of the geometrical parameters and the roughness parameters on the thermal conductivity are investigated in this section. Finally, in Section IV a summary and concluding remarks are presented.

II. MODEL AND METHOD

In narrow AGNRs, LER is the dominant scattering source for phonon transport [34], [40]. Very recently, the effect of rough boundaries is studied in defective AGNRs [32]–[37]. Those previous works have used a simple model for LER which neglect the correlation of the roughness. However, because of the wave nature of phonons, correlation length of roughness plays an important role as well. To model LER-limited thermal conductivity, an exponential autocorrelation function is employed [41]

$$R(x) = \Delta W^2 \exp\left(-\frac{|x|}{\Delta L}\right) \quad (1)$$

the Fourier transform of which is the power spectrum of the roughness. In (1), ΔW is the rms of the roughness amplitude and ΔL is the roughness correlation length. The LER in the real space is achieved by adding a random phase to the power spectrum followed by an inverse Fourier transform [1], [41]. We have recently employed this model to rigorously study the role of geometrical and roughness parameters on the electronic transport of rough AGNRs [1], [29]. Similar to our previous work many samples with the same roughness parameters are generated and their thermal properties are evaluated by considering an ensemble average. The contacts are assumed to be semi infinite pristine ribbons and the LER is introduced in the channel part only. In such structure, the calculated thermal properties arise from the channel part of the device only [42]. To study the transport of phonons an atomistic nonequilibrium Green's function method is used in this paper. The device Green's function is obtained as [43], [44]

$$G(E) = \left(E^2 I - D - \Sigma_s - \Sigma_d\right)^{-1} \quad (2)$$

where D is device dynamical matrix and $E = \hbar\omega$ is the phonon energy. The dynamical matrix is setup using a fourth nearest neighbor force constant approximation as described in [42], [45]. The contact self-energy matrices $\Sigma_{s,d}$ are calculated using the Sancho-Rubio iterative scheme [46]. The effective transmission probability through the channel is given by the following:

$$\overline{T}_{\text{ph}}(E) = \text{Trace}[\Gamma_1 G \Gamma_2 G^\dagger] \quad (3)$$

where Γ_1 and Γ_2 are the broadening functions of the two contacts [44].

According to the Landauer formalism, heat current can be evaluated from the electron and phonon transmission probabilities. In the linear response regime, one can express the lattice thermal conductance as [23], [47]

$$K_l = \left(\frac{k_B^2 T \pi^2}{3h}\right) \int_0^{+\infty} \overline{T}_{\text{ph}}(\omega) W_{\text{ph}}(\hbar\omega) d(\hbar\omega) \quad (4)$$

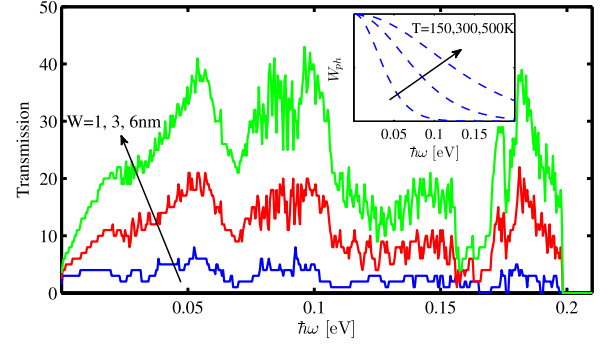


Fig. 1. Ballistic transmission of phonons in AGNRs of widths 1, 3, and 6 nm. Inset: phononic window function at $T = 150, 300, 500$ K.

where the phononic window function is given by the following:

$$W_{\text{ph}}(\hbar\omega) = \frac{3}{\pi^2} \left(\frac{\hbar\omega}{k_B T}\right)^2 \frac{\partial n(\hbar\omega)}{\partial(\hbar\omega)}. \quad (5)$$

Here, $n(\omega)$ denotes the Bose-Einstein distribution function. The lattice thermal conductivity is given by the following:

$$\kappa_l = K_l \frac{L}{WH} \quad (6)$$

where L is the channel length, W is the ribbon's width, and $H = 0.335$ nm is the effective thickness of the graphene monolayer [48], [49].

III. RESULTS AND DISCUSSION

In this section, the role of geometrical and roughness parameters on the phonon transport in AGNRs is studied. The ribbon's width varies between 1 nm and 10 nm. This corresponds to AGNRs with 7, 16, 25, 31, 40, 49, and 80 indices. Channel lengths up to 40 nm are studied. The maximum roughness amplitude is chosen to be 10% of ribbons' width, and the correlation lengths varies between 1 nm and 10 nm. The diffusive thermal conductivity is extracted from the results as well.

A. Ballistic Properties

The ballistic transmission function of phonons, which is the number of phononic channels at some energy $\hbar\omega$, is shown in Fig. 1. As expected, the transmission function increases with the ribbon's width. In addition, the phononic window function is shown in the inset of Fig. 1 at various temperatures. This function, which qualifies the contribution of different phonon frequencies in the thermal conductance, increases with temperature. Therefore, at higher temperatures high energy phonons contribute to the thermal transport as well.

Fig. 2 shows the ballistic thermal conductance of AGNRs as a function of temperature and the ribbon's width. By increasing the temperature and thus the phononic window function, the thermal conductance increases. However, as the energy spectrum of AGNRs is limited to 0.2 eV (Fig. 1), the thermal conductance saturates at very high temperatures ($\sim T > 800$ K). As shown in Fig. 2(b), the thermal conductance increases linearly with the ribbon's width. The ballistic thermal conductance divided by the width is

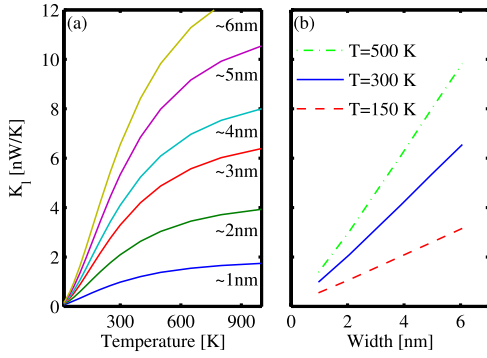


Fig. 2. Ballistic lattice thermal conductance of AGNRs at various widths as a function of (a) temperature and (b) width.

constant. This is because of the fact that by increasing the width and thus the number of carbon atoms in the unit cell, the number of modes increases almost linearly in the whole energy spectrum, and, therefore, the ballistic transmission function is directly proportional to the width.

On the other hand, a high thermal conductivity in the range of $\sim 2000\text{--}5300$ W/mK is reported for suspended single-layer graphene [16], [50], which is only weakly affected by the boundary and substrate scatterings. Using this superior thermal conductivity a phonon mean-free-path (MFP) of ~ 775 nm is extracted [2]. Because of this relatively large MFP, no saturation is observed in the thermal conductivity of short ribbons with smooth edges [51]. When the MFP is large enough the conductivity is mostly determined by the channel length (6) rather than phonon scattering. In the next section we examine how the LER scattering in very narrow AGNRs can drastically decrease the MFP, which can significantly affect the length dependence of the thermal conductivity.

B. Role of Channel Length

To investigate the effect of LER on the thermal conductivity and the MFP, we performed simulations on a statistical sample of 16-AGNR with roughness parameters of $\Delta W = 0.1$ nm and $\Delta L = 2$ nm. The statistical average of the transmission function is shown in Fig. 3 for channel lengths of 5 nm and 40 nm. For reference, the ballistic transmission of 16-AGNR is also shown in black color.

Fig. 3 shows the transmission functions of 16-AGNR assuming perfect edges and rough edges with roughness parameters of $\Delta W = 0.1$ nm and $\Delta L = 2$ nm. Apparently, increasing the length decreases the transmission function. To quantify the dependence of the transmission function on the channel length, the phonon MFP is defined as [44], [52]

$$\bar{T}_{\text{ph}}(\hbar\omega) = \frac{N_{\text{ph}}(\hbar\omega)}{1 + L/\lambda_{\text{ph}}(\hbar\omega)} \quad (7)$$

where $N_{\text{ph}}(\hbar\omega)$ is the ballistic transmission function and $\lambda_{\text{ph}}(\hbar\omega)$ is the phonon MFP at energy $\hbar\omega$. In the inset of Fig. 4(a), the transmission function of 16-AGNR at $\hbar\omega = 50$ meV is shown as a function of the channel length. The extracted MFP at this phonon energy is about 7 nm. Fig. 4(a) shows that the MFP is smaller than 30 nm in most of

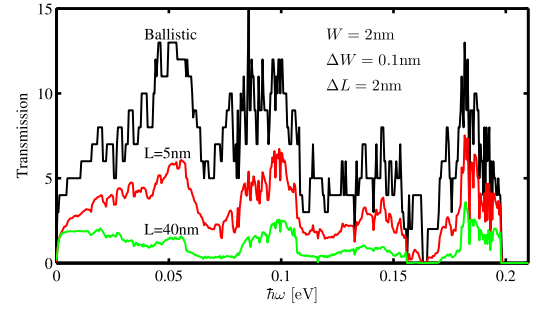


Fig. 3. Transmission function for 16-AGNR: Ballistic result (black); in the presence of LER with $\Delta W = 0.1$ nm and $\Delta L = 2$ nm for channel lengths of 5 nm (red) and 40 nm (green). Increasing the length decreases the transmission function of the rough ribbons.

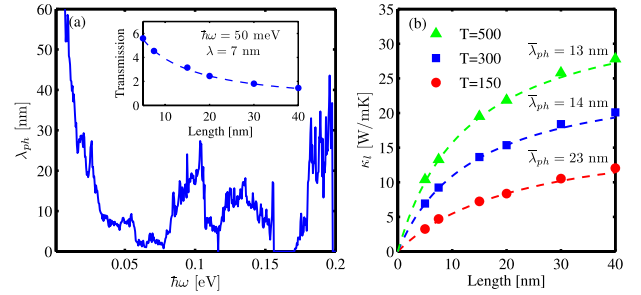


Fig. 4. (a) LER-limited MFP of 16-AGNR for $\Delta W = 0.1$ nm and $\Delta L = 2$ nm as a function of phonon energy. Inset: transmission function at $\hbar\omega = 50$ meV as a function of the channel length. Its corresponding MFP is about 7 nm. (b) Lattice thermal conductivity as a function of the channel length. Using (9) with $L_1 = 5$ nm and $L_2 = 20$ nm, the effective MFPs are extracted as 23, 14, and 13 nm at $T = 150, 300,$ and 500 K, respectively. The dashed lines are plotted based on (9), $L_1 = 5$ nm, and varying L_2 as the channel length.

the spectrum, except at very low frequencies. The length dependence of the lattice thermal conductivity of this ribbon is shown in Fig. 4(b). In contrast to the ribbons with smooth edges, here the thermal conductivity increases with length and starts to saturate above $L = 40$ nm. The symbols in Fig. 4(b) are ensemble average values, however, the numerical results show a standard deviation of $\sim 0.5\text{--}1.0$ W/mK in the thermal conductivity. As a rough estimate, the standard deviations of various quantities calculated in this paper are about 10% of the corresponding average value for short and narrow channels, whereas they decrease to $\sim 5\%$ of the average values for long and wide channel. To study the dependence of the thermal conductance on the channel length one can define an effective MFP $\bar{\lambda}_{\text{ph}}$ as [13]

$$\kappa_l = \kappa_{l,B} \frac{\bar{\lambda}_{\text{ph}}}{L + \bar{\lambda}_{\text{ph}}} \quad (8)$$

which covers the contribution of phonons of different frequencies. The ballistic thermal conductance of AGNRs with perfect edges is denoted by $\kappa_{l,B}$. Alternatively, the effective MFP can be expressed as follows:

$$\frac{\kappa_l(L_1)}{\kappa_l(L_2)} = \frac{L_1 \bar{\lambda}_{\text{ph}} + L_2}{L_2 \bar{\lambda}_{\text{ph}} + L_1} \quad (9)$$

which makes the numerical calculation more tractable. In Fig. 4(b), using (9) with $L_1 = 5$ nm and $L_2 = 20$ nm, the

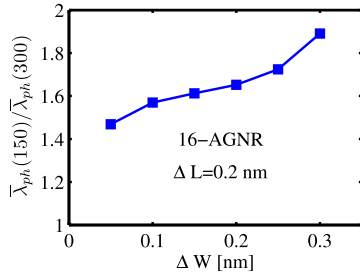


Fig. 5. Ratio of effective MFPs at $T = 150$ and $T = 300$ K.

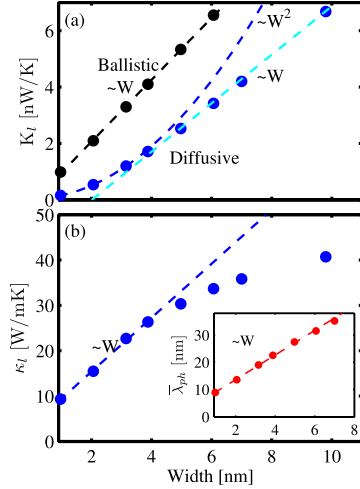


Fig. 6. (a) Thermal conductance and (b) thermal conductivity as a function of the ribbon's width at room temperature. Inset: phonon MFP scales linearly with the ribbon's width. The parameters are $\Delta W = 0.1$ nm, $\Delta L = 2$ nm, and $L = 20$ nm. The dashed lines are guides to the eye.

effective MFPs are extracted as 23, 14, and 13 nm at $T = 150$, 300, and 500 K, respectively. The dashed lines are plotted based on (9), $L_1 = 5$ nm, and varying L_2 as the channel length. The effective MFP is high at low temperatures because at low temperatures thermal transport is dominated by low frequency phonons that have longer MFPs [see Fig. 4(a)]. Low frequency phonons with long-wavelengths undergo mostly specular scattering on the boundaries [53]. As shown in Fig. 5, the ratio of the effective MFPs at $T = 150$ K and $T = 300$ K increases with the roughness amplitude, indicating that short-length roughness affects the transport of short-wavelength phonons more than that of long-wave phonons. However, in the rest of this paper we consider only the room-temperature operation.

C. Role of Ribbon's Width

The lattice thermal conductance as a function of width in the presence of LER with $\Delta W = 0.1$ nm and $\Delta L = 2$ nm is shown in Fig. 6(a). The ballistic conductance is proportional to the ribbon's width. In the presence of roughness, the thermal conductance is smaller than the ballistic one. It increases quadratically with W for narrow ribbons and then a linear increase is observed. This behavior can be understood by considering the fact that effective MFP increases with ribbon's width [inset of Fig. 6(b)]. Therefore, in wide ribbons, the MFP

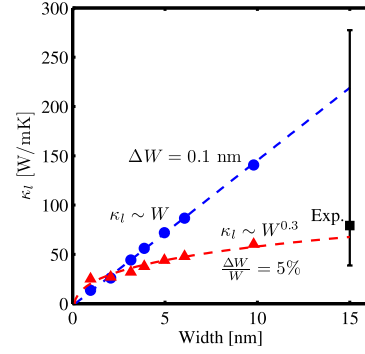


Fig. 7. Room temperature diffusive lattice thermal conductivity as a function of width. A constant roughness amplitude ($\Delta W = 0.1$ nm) and a constant relative roughness ($\Delta W/W = 5\%$) are considered. The roughness correlation length is $\Delta L = 2$ nm. The dashed lines are fitted based on the least mean square error. Experimental data is taken from [40].

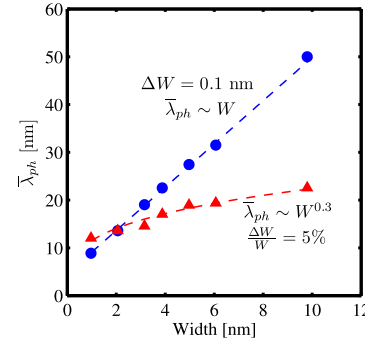


Fig. 8. Room temperature effective phonon MFP as a function of the ribbon's width. Both a constant roughness amplitude ($\Delta W = 0.1$ nm) and a constant relative roughness ($\Delta W/W = 5\%$) are considered. The roughness correlation length is $\Delta L = 2$ nm. The dashed lines are fitted based on the least mean square error.

is larger than the channel length $L = 20$ nm. According to (8) the conductance is proportional to the ballistic conductance that scales linearly with the ribbon's width. On the other hand, for narrow ribbons, the MFP in the denominator of (8) is negligible in comparison with the channel length L , such that $K_l \sim K_{l,B} \bar{\lambda}_{ph}$, and as a result $K_l \sim W^2$. Therefore, the thermal conductivity ($\sim K_l/W$) saturates for wide ribbons and the feature of constant ballistic thermal conductance per unit width [see Fig. 2(b)] is observed in the thermal conductivity.

When the channel length is larger than the MFP, the purely diffusive thermal conductivity, which is length independent, can be extracted using (9). The diffusive thermal conductivity as a function of ribbon's width is shown in Fig. 7 for two cases of constant roughness amplitude and constant relative roughness. The experimental result is taken from [40]. The results indicate that a relative roughness between $\sim 0.5\%$ and $\sim 5\%$ can cover the range of the experimental data. It is, however, worth mentioning that the experimental data is for rough GNRs supported by SiO_2 substrates. However, as shown in [37], phonon transport in narrow GNRs ($W < 130$ nm) is limited by LER, indicating that the distinction is expected to be negligible. In the case of fixed roughness amplitude, the diffusive thermal conductivity is proportional to the ribbon's width, similar to the effective MFP [inset of Fig. 6(b)], implying that

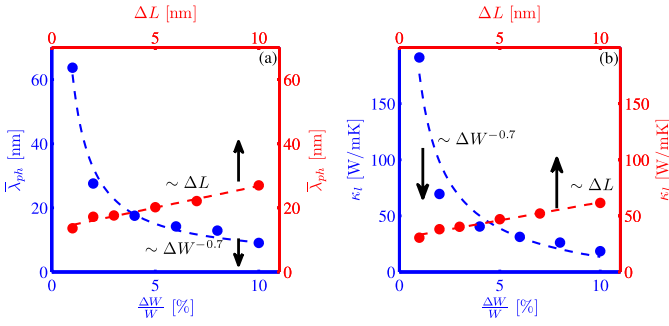


Fig. 9. (a) Room temperature effective MFP and (b) diffusive thermal conductivity of 25 AGNR as a function of relative roughness and correlation length. For ΔL -varying curves $\Delta W/W = 4\%$ and for $\Delta W/W$ -varying curves $\Delta L = 3$ nm. The dashed lines are fitted based on the least mean square error.

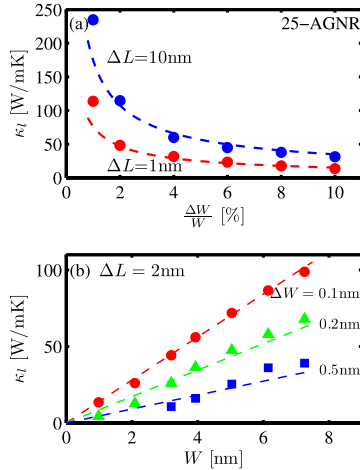


Fig. 10. Room temperature diffusive lattice thermal conductivity of (a) 25 AGNR at various roughness parameters and (b) different widths as well as various roughness amplitude. The dashed lines are the fitted curves based on (10) and symbols indicate the numerical results.

the LER relaxation time is proportional to W as proposed in the conventional formula for boundary scattering [36], [53]. On the other hand, at fixed relative roughness, the diffusive thermal conductivity is only weakly dependent on the width ($\sim W^{0.3}$). This behavior can be understood by considering the dependence of the effective MFP on the roughness amplitude. As shown in Fig. 8 the effective MFP is weakly related to the ribbon's width, $\sim W^{0.3}$, at fixed relative roughness amplitude. However, at fixed roughness amplitude it scales linearly with the width.

D. Role of Roughness Parameters

Fig. 9 shows that both the effective MFP and the diffusive thermal conductivity are inversely proportional to the relative roughness amplitude and scale linearly with the correlation length. It is worth mentioning that the roughness parameters change at fixed width, in contrast to Fig. 8. Although the relative roughness amplitude affect the thermal conductivity stronger than the roughness correlation length, at large roughness amplitude the role of correlation length will be as important as the relative roughness amplitude. As described in Section III-C, the thermal conductivity depends to the rel-

ative roughness rather than the absolute roughness amplitude. Therefore, we propose the following model for the diffusive lattice thermal conductivity at room temperature:

$$\kappa_l = (a + b\Delta L) \frac{W}{\Delta W^{0.7}}. \quad (10)$$

The best fit to the numerical results is achieved for $a = 2.1$, and $b = 0.35$, where W , ΔW , and ΔL are expressed in [nm]. Fig. 10 compares the thermal conductivity obtained from numerical simulations with the analytical model proposed in (10) at various geometrical and roughness parameters. Excellent agreement shows the usefulness of the proposed model for accurate analysis of the thermal properties of GNR-based devices.

IV. CONCLUSION

Using an atomistic LER model along with the nonequilibrium Green's function technique, the thermal properties of AGNRs less than 10 nm wide were comprehensively studied and modeled. The results indicated that besides geometrical parameters (width and length) the roughness parameters played an important role in thermal transport as well. The results indicated that the diffusive thermal conductivity was proportional to the ribbon's width and the roughness correlation length, and inversely proportional to the roughness amplitude. Therefore, a short ribbon with small roughness amplitude and long roughness correlation length was appropriate for thermal management, whereas a long ribbon with short correlation length and large roughness amplitude was more appropriate for thermoelectric applications.

REFERENCES

- [1] A. Yazdanpanah, M. Pourfath, M. Fathipour, H. Kosina, and S. Selberherr, "A numerical study of line-edge roughness scattering in graphene nanoribbons," *IEEE Trans. Electron Devices*, vol. 59, no. 2, pp. 433–440, Feb. 2012.
- [2] S. Ghosh, I. Calizo, D. Teweldebrahn, E. Pokatilov, D. Nika, A. Balandin, W. Bao, F. Miao, and C. Lau, "Extremely high thermal conductivity of graphene: Prospects for thermal management applications in nanoelectronic circuits," *Appl. Phys. Lett.*, vol. 92, pp. 151911-1–151911-3, May 2008.
- [3] A. Majumdar, "Thermoelectric devices: Helping chips to keep their cool," *Nature Nanotechnol.*, vol. 4, no. 4, pp. 214–215, 2009.
- [4] R. Venkatasubramanian, E. Siivola, T. Colpitts, and B. O'Quinn, "Thin-film thermoelectric devices with high room-temperature figures of merit," *Nature*, vol. 413, no. 6856, pp. 597–602, 2001.
- [5] T. Harman, P. Taylor, M. Walsh, and B. LaForge, "Quantum dot superlattice thermoelectric materials and devices," *Science*, vol. 297, no. 5590, pp. 2229–2232, 2002.
- [6] K. Novoselov, A. Geim, S. Morozov, D. Jiang, Y. Zhang, S. Dubonos, and I. Grigorieva, "Electric field effect in atomically thin carbon films," *Science*, vol. 306, pp. 666–669, Oct. 2004.
- [7] M. Liu, X. Yin, E. Ulin-Avila, B. Geng, T. Zentgraf, L. Ju, F. Wang, and X. Zhang, "A graphene-based broadband optical modulator," *Nature*, vol. 474, pp. 64–67, Jun. 2011.
- [8] S. Yuan, R. Roldan, H. Raedt, and M. Katsnelson, "Optical conductivity of disordered graphene beyond the dirac cone approximation," *Phys. Rev. B*, vol. 84, no. 19, pp. 195418-1–195418-11, 2011.
- [9] G. Fiori and G. Iannaccone, "Simulation of graphene nanoribbon field-effect transistors," *IEEE Electron Device Lett.*, vol. 28, no. 8, pp. 760–762, Aug. 2007.
- [10] D. Basu, M. Gilbert, L. Register, S. Banerjee, and A. MacDonald, "Effect of edge roughness on electronic transport in graphene nanoribbon channel metal-oxide-semiconductor field-effect transistors," *Appl. Phys. Lett.*, vol. 92, no. 4, pp. 042114-1–042114-3, 2008.

- [11] Y. M. Zuev, W. Chang, and P. Kim, "Thermoelectric and magnetothermoelectric transport measurements of graphene," *Phys. Rev. Lett.*, vol. 102, no. 9, pp. 096807-1–096807-4, 2009.
- [12] P. Wei, W. Bao, Y. Pu, C. N. Lau, and J. Shi, "Anomalous thermoelectric transport of dirac particles in graphene," *Phys. Rev. Lett.*, vol. 102, no. 6, pp. 166808-1–166808-4, 2009.
- [13] H. Sevincli and G. Cuniberti, "Enhanced thermoelectric figure of merit in edge-disordered zigzag graphene nanoribbons," *Phys. Rev. B*, vol. 81, no. 11, pp. 113401-1–113401-4, 2010.
- [14] H. Karamitaheri, N. Neophytou, M. Pourfath, R. Faez, and H. Kosina, "Engineering enhanced thermoelectric properties in zigzag graphene nanoribbons," *J. Appl. Phys.*, vol. 111, no. 5, pp. 054501-1–054501-9, 2012.
- [15] J. Hone, M. Whitney, C. Piskoti, and A. Zettl, "Thermal conductivity of single-walled carbon nanotubes," *Phys. Rev. B*, vol. 59, no. 4, pp. R2514–R2516, 1999.
- [16] A. Balandin, S. Ghosh, W. Bao, I. Calizo, D. Teweldebrhan, F. Miao, and C. Lau, "Superior thermal conductivity of single-layer graphene," *Nano Lett.*, vol. 8, no. 3, pp. 902–907, 2008.
- [17] A. A. Balandin, "Thermal properties of graphene and nanostructured carbon materials," *Nature Mater.*, vol. 10, pp. 569–581, Jul. 2011.
- [18] D. Nika and A. Balandin, "Two-dimensional phonon transport in graphene," *J. Phys., Condensed Matter*, vol. 24, no. 23, p. 233203, 2012.
- [19] J. Seol, I. Jo, A. Moore, L. Lindsay, Z. Aitken, M. Pettes, X. Li, Z. Yao, R. Huang, D. Broid, N. Mingo, R. Ruoff, and L. Shi, "Two-dimensional phonon transport in supported graphene," *Science*, vol. 328, no. 5975, pp. 213–216, 2010.
- [20] M. Han, B. Ozyilmaz, Y. Zhang, and P. Kim, "Energy band-gap engineering of graphene nanoribbons," *Phys. Rev. Lett.*, vol. 98, no. 20, pp. 206805-1–206805-4, 2007.
- [21] A. Zhang, H. Teoh, Z. Dai, Y. Feng, and C. Zhang, "Intrinsic and extrinsic performance limits of graphene devices on SiO₂," *Appl. Phys. Lett.*, vol. 98, pp. 023105-1–023105-3, Sep. 2011.
- [22] H. Karamitaheri, M. Pourfath, R. Faez, and H. Kosina, "Geometrical effects on the thermoelectric properties of ballistic graphene antidot lattices," *J. Appl. Phys.*, vol. 110, no. 5, pp. 054506-1–054506-6, 2011.
- [23] Y. Ouyang and J. Guo, "A theoretical study on thermoelectric properties of graphene nanoribbons," *Appl. Phys. Lett.*, vol. 94, no. 26, pp. 263107-1–263107-3, 2009.
- [24] D. Areshkin, D. Gunlycke, and C. White, "Ballistic transport in graphene nanostrips in the presence of disorder: Importance of edge effects," *Nano Lett.*, vol. 7, no. 1, pp. 204–210, 2007.
- [25] J.-W. Jiang, B.-S. Wang, and J.-S. Wang, "First principle study of the thermal conductance in graphene nanoribbon with vacancy and substitutional silicon defects," *Appl. Phys. Lett.*, vol. 98, no. 11, pp. 113114-1–113114-3, 2011.
- [26] J. Hu, S. Schiffl, A. Vallabhaneni, X. Ruan, and Y. Che, "Tuning the thermal conductivity of graphene nanoribbons by edge passivation and isotope engineering: A molecular dynamics study," *Appl. Phys. Lett.*, vol. 97, no. 13, pp. 133107-1–133107-3, 2010.
- [27] P. Zhao and J. Guo, "Modeling edge effects in graphene nanoribbon field-effect transistors with real and mode space methods," *J. Appl. Phys.*, vol. 105, no. 3, pp. 034503-1–034503-7, 2009.
- [28] A. Yazdanpanah, M. Pourfath, M. Fathipour, H. Kosina, and S. Selberherr, "An analytical model for line-edge roughness limited mobility of graphene nanoribbons," *IEEE Trans. Electron Devices*, vol. 58, no. 11, pp. 3725–3735, Nov. 2011.
- [29] A. Yazdanpanah, M. Pourfath, M. Fathipour, and H. Kosina, "Device performance of graphene nanoribbon field-effect transistors in the presence of line-edge roughness," *IEEE Trans. Electron Devices*, vol. 59, no. 12, pp. 3527–3532, Dec. 2012.
- [30] N. D. Akhavan, G. Jolley, G. A. Umana-Membreno, J. Antoszewski, and L. Faraone, "Phonon limited transport in graphene nanoribbon field effect transistors using full three dimensional quantum mechanical simulation," *J. Appl. Phys.*, vol. 112, no. 9, pp. 094505-1–094505-11, 2012.
- [31] M. Pourfath and H. Kosina, "Fast convergent Schrodinger-Poisson solver for the static and dynamic analysis of carbon nanotube field effect transistors," in *Large-Scale Scientific Computing* (Lecture Notes in Computer Science), vol. 3743. Berlin, Germany: Springer-Verlag, 2006, pp. 578–585.
- [32] Y. A. Kosevich and A. V. Savin, "Reduction of phonon thermal conductivity in nanowires and nanoribbons with dynamically rough surfaces and edges," *Europhys. Lett.*, vol. 88, no. 1, p. 14002, 2009.
- [33] D. L. Nika, E. P. Pokatilov, A. S. Askerov, and A. A. Balandin, "Phonon thermal conduction in graphene: Role of Umklapp and edge roughness scattering," *Phys. Rev. B*, vol. 79, no. 15, pp. 155413-1–155413-12, 2009.
- [34] W. Evans, L. Hu, and P. Keblinski, "Thermal conductivity of graphene ribbons from equilibrium molecular dynamics: Effect of ribbon width, edge roughness, and hydrogen termination," *Appl. Phys. Lett.*, vol. 96, no. 20, pp. 203112-1–203112-3, 2010.
- [35] A. Savin, Y. Kivshar, and B. Hu, "Suppression of thermal conductivity in graphene nanoribbons with rough edges," *Phys. Rev. B*, vol. 82, no. 19, pp. 195422-1–195422-9, 2010.
- [36] Z. Aksamija and I. Knezevic, "Lattice thermal conductivity of graphene nanoribbons: Anisotropy and edge roughness scattering," *Appl. Phys. Lett.*, vol. 98, no. 14, pp. 141919-1–141919-3, 2011.
- [37] Z. Aksamija and I. Knezevic, "Thermal transport in graphene nanoribbons supported on SiO₂," *Phys. Rev. B*, vol. 86, no. 6, pp. 165426-1–165426-6, 2012.
- [38] J. Lim, K. Hippalgaonkar, S. C. Andrews, A. Majumdar, and P. Yang, "Quantifying surface roughness effects on phonon transport in silicon nanowires," *Nano Lett.*, vol. 12, no. 5, pp. 2475–2482, 2012.
- [39] J. P. Feser, J. S. Sadhu, B. P. Azeredo, K. H. Hsu, J. Ma, J. Kim, M. Seong, N. X. Fang, X. Li, P. M. Ferreira, S. Sinha, and D. G. Cahill, "Thermal conductivity of silicon nanowire arrays with controlled roughness," *J. Appl. Phys.*, vol. 112, no. 11, pp. 114306-1–114306-7, 2012.
- [40] A. D. Liao, J. Z. Wu, X. Wang, K. Tahy, D. Jena, H. Dai, and E. Pop, "Thermally limited current carrying ability of graphene nanoribbons," *Phys. Rev. Lett.*, vol. 106, no. 25, pp. 256801-1–256801-4, 2011.
- [41] J. Wu, "Simulation of non-Gaussian surfaces with FFT," *Tribol. Int.*, vol. 37, no. 4, pp. 339–346, 2004.
- [42] H. Karamitaheri, N. Neophytou, M. Pourfath, and H. Kosina, "Study of thermal properties of graphene-based structures using the force constant method," *J. Comp. Electron.*, vol. 11, no. 1, pp. 14–21, 2012.
- [43] W. Zhang, T. Fisher, and N. Mingo, "The atomistic Green's function method: An efficient simulation approach for nanoscale phonon transport," *Numer. Heat Transf., B, Fundam., Int. J. Comput. Methodol.*, vol. 51, no. 4, pp. 333–349, 2007.
- [44] S. Datta, *Quantum Transport: Atom to Transistor*. Cambridge: Cambridge Univ. Press, 2005.
- [45] R. Saito, M. Dresselhaus, and G. Dresselhaus, *Rysical Properties of Carbon Nanotubes*. London, U.K.: Imperial College Press, 1998.
- [46] M. Sancho, J. Sancho, J. Sancho, and J. Rubio, "Highly convergent schemes for the calculation of bulk and surface green functions," *J. Phys. F, Metal Phys.*, vol. 15, no. 4, pp. 851–858, 1985.
- [47] C. Jeong, S. Datta, and M. Lundstrom, "Full dispersion versus debye model evaluation of lattice thermal conductivity with a Landauer approach," *J. Appl. Phys.*, vol. 109, no. 7, pp. 073718-1–073718-8, 2011.
- [48] R. Al-Jishi and G. Dresselhaus, "Lattice-dynamical model for graphite," *Phys. Rev. B*, vol. 26, no. 8, pp. 4514–4522, 1982.
- [49] C. Lee, X. Wei, J. W. Kysar, and J. Hone, "Measurement of the elastic properties and intrinsic strength of monolayer graphene," *Science*, vol. 321, no. 5887, pp. 385–388, 2008.
- [50] D. L. Nika, A. S. Askerov, and A. A. Balandin, "Anomalous size dependence of the thermal conductivity of graphene ribbons," *Nano Lett.*, vol. 12, no. 6, pp. 3238–3244, 2012.
- [51] Z. Guo, D. Zhang, and X.-G. Gong, "Thermal conductivity of graphene nanoribbons," *Appl. Phys. Lett.*, vol. 95, no. 16, pp. 163103-1–163103-3, 2009.
- [52] C. Jeong, S. Datta, and M. Lundstrom, "Thermal conductivity of bulk and thin-film silicon: A Landauer approach," *J. Appl. Phys.*, vol. 111, no. 9, pp. 093708-1–093708-6, 2012.
- [53] J. M. Ziman, *Electrons and Phonons: The Theory of Transport Phenomena in Solids*. London, U.K.: Oxford Univ. Press, 1960.